Coherence length of an elongated condensate

A study by matter-wave interferometry

M. Hugbart[1,a], J.A. Retter[1], F. Gerbier[2], A.F. Varón[1], S. Richard[3], J.H. Thywissen[4], D. Clément[1],
P. Bouyer[1], and A. Aspect[1]

1 Laboratoire Charles Fabry de l'Institut d'Optique, UMR8501 du CNRS, 91403 Orsay Cedex, France
2 Institut für Physik, Johannes Gutenberg Universität, Staudingerweg 7, 55099 Mainz, Germany
3 THALES Research & Technology, 91404 Orsay Cedex, France
4 Department of Physics, University of Toronto, 60 Saint George St, Toronto, Ontario, M5S 1A7 Canada

Abstract. We measure the spatial correlation function of Bose-Einstein condensates in the cross-over region
between phase-coherent and strongly phase-fluctuating condensates. We observe the continuous path from
a Gaussian-like shape to an exponential-like shape characteristic of one-dimensional phase-fluctuations.
The width of the spatial correlation function as a function of the temperature shows that the condensate
coherence length undergoes no sharp transition between these two regimes.

PACS. 03.75.Hh Static properties of condensates; thermodynamical, statistical and structural properties –
03.75.Dg Atom and neutron interferometry – 39.20.+q Atom interferometry techniques

1 Introduction

The high atomic phase-space density provided by a
Bose-Einstein condensate (BEC) [1] has driven interest
in guiding atoms in a manner analogous to guiding laser
light through single-mode optical fibres. The most ad-
vanced technology to date is based on *atom chips*, where
the fields which trap and guide the atoms are created by
microfabricated structures [2–7]. Many groups around the
world have already succeeded in preparing BEC on an
atom chip [8–14] and one can envisage using this technol-
ogy to create integrated atom interferometers [15–18]. In
this context, a precise characterization of the phase coher-
ence properties of the condensate is crucial [19–21].

Trapping quantum gases on atom chips naturally in-
volves highly elongated, guide-like traps. Changing the di-
mensionality of the system from three-dimensional (3D)
towards one-dimensional (1D) has a profound effect on the
phase coherence of the condensate. In 3D condensates of
modest aspect ratio, experimental results show that phase
coherence extends across the whole cloud [22,23], even at
finite temperature [24]. However, in the 1D regime, ther-
mal excitations of the low energy axial modes lead to phase
fluctuations which degrade the phase coherence [25,26].
Condensates exhibiting such phase fluctuations are known
as *quasi-condensates*.

In the intermediate regime of elongated 3D conden-
sates with a high aspect ratio, a behaviour similar to the

1D case is observed [27]: below a characteristic tempera-
ture T_ϕ determined by the atom number and the trapping
frequencies, the condensate is nearly phase coherent, but
above T_ϕ the population of the axial modes is high and
phase fluctuations may be pronounced. For weakly elon-
gated condensates, T_ϕ can be higher than the transition
temperature T_c, so that the condensate is nearly phase
coherent at all temperatures. In contrast, atom chips can
easily produce traps with high aspect ratios ($\sim$1000) for
which T_ϕ can be much smaller than T_c. Phase fluctuations
are therefore likely to impose limits on the performance
of atom chip devices and need to be well understood.

In an elongated condensate, the wavelength of the low
energy axial modes is longer than the radial size of the
condensate, so these excitations have a 1D character. How-
ever, the wavelength of these excitations can be much
shorter than the axial length of the condensate, reducing
the phase coherence length in the axial direction. An im-
portant feature of quasi-condensates is that density fluc-
tuations remain suppressed in the trap, due to the mean
field energy, even in the presence of large phase fluctua-
tions [21,27]. Therefore, the 3D quasi-condensate has the
usual parabolic profile in the Thomas-Fermi limit.

Phase-fluctuating condensates in elongated traps were
first observed by the conversion of phase fluctuations
into density fluctuations after a sufficiently long free
expansion [19] and by a condensate-focussing tech-
nique [20]. Quantitative measurements of the phase coher-
ence length have since been obtained from the momentum

a e-mail: mathilde.hugbart@iota.u-psud.fr

distribution [21] and the second-order correlation function [28]. The results of each of these experiments showed good agreement with theory [27] in the strongly phase-fluctuating regime (at temperatures $T \gg T_\phi$). However, neither experiment explored the cross-over region ($T \sim T_\phi$) between phase-coherent and strongly phase-fluctuating condensates.

In this article we describe a new experiment using a matter-wave interferometer and Fourier-space analysis to measure the spatial correlation function, thereby extending our measurements into the cross-over region ($T \sim T_\phi$). Our results agree with the predicted shapes of the correlation function: for $T \gg T_\phi$, we find exponential-like correlation functions as predicted for significant phase fluctuations, whereas at $T \sim T_\phi$ we find a Gaussian-like shape, as expected when the phase profile is nearly flat and the correlation function decay is dominated by the density profile. The coherence length as a function of T/T_ϕ follows the trend predicted by theory, showing that the coherence length increases smoothly as the temperature falls and that there is no sharp transition at T_ϕ. This highlights the fact that phase fluctuations occur at all finite temperatures, even if these effects are too small to be resolved experimentally for more spherical traps. However, whereas our previous measurements based on momentum spectroscopy [21], realized for high T/T_ϕ, were in full agrement with the theory, two observations remain unexplained in the interferometric method. First, as in a previous experiment [22], our experimental measurements of the coherence length are shifted from the theoretical prediction, by about 25% for $T/T_\phi = 1$, even after taking the limitations of our imaging system into account. Second, our interferometer produces unexplained supplementary fringes outside of the region where the condensates overlap, and we note that similar unexplained fringes appear in other published data [29]. These supplementary fringes do not seem to be compatible with interference of the thermal cloud observed in [30].

2 Measurement of the coherence length by atom interferometry

A natural method to study the coherence length along the long axis z of a condensate, or a quasi-condensate, is to use atom interferometry. With atomic beam-splitters, one produces two daughter copies of the initial condensate with a separation s, and observes the interference pattern appearing in the atomic density:

$$
\begin{aligned}
n(\mathbf{r}) &\propto \left| \Psi_0 \left(\mathbf{r} - \frac{s}{2}\mathbf{e}_z \right) + e^{i\phi_{\mathrm{rel}}} \Psi_0 \left(\mathbf{r} + \frac{s}{2}\mathbf{e}_z \right) \right|^2 \\
&\propto \left| \Psi_0 \left(\mathbf{r} - \frac{s}{2}\mathbf{e}_z \right) \right|^2 + \left| \Psi_0 \left(\mathbf{r} + \frac{s}{2}\mathbf{e}_z \right) \right|^2 \\
&\quad + 2\mathrm{Re} \left[e^{i\phi_{\mathrm{rel}}} \Psi_0^* \left(\mathbf{r} - \frac{s}{2}\mathbf{e}_z \right) \Psi_0 \left(\mathbf{r} + \frac{s}{2}\mathbf{e}_z \right) \right], \quad (1)
\end{aligned}
$$

where $\mathbf{e}_z$ is the axial unit vector, $\Psi_0(\mathbf{r})$ is the wavefunction describing the initial condensate and ϕ_{rel} a relative phase

shift produced by the interferometer and the free fall of the condensate.

Let us first consider the behaviour of a fully phase coherent condensate. During free expansion, it acquires a phase distribution proportional to z^2 [31]. The phase difference ϕ_{rel} between two displaced copies of the condensate is therefore proportional to zs, giving rise to an interference pattern of straight fringes, uniformly spaced along the longitudinal direction, the spatial frequency of the fringes being proportional to the separation s. The fringe contrast integrated over the entire condensate gives the first-order correlation function at s:

$$
C^{(1)}(s) = \int \mathrm{d}^3\mathbf{r}\, \Psi_0^* \left(\mathbf{r} - \frac{s}{2}\mathbf{e}_z \right) \Psi_0 \left(\mathbf{r} + \frac{s}{2}\mathbf{e}_z \right). \quad (2)
$$

Repeating this contrast measurement for different separations s, one can study the decay of $C^{(1)}(s)$ with increasing s [22]. For a fully phase coherent condensate, the first-order correlation function decay reflects only the width of the density profile $n(\mathbf{r})$ [32].

In the case of a quasi-condensate, 1D thermal excitations cause the phase to fluctuate along the longitudinal axis, both spatially and temporally. In our experiment, these fluctuations are small compared to the parabolic phase developed during free expansion. Therefore when we image the overlapping condensates after free expansion, we still observe straight fringes, but they are no longer strictly periodic. Small local phase shifts add a "jitter" to the fringe spacing, which in Fourier space has the effect of broadening the peak at the spatial frequency of the fringes and thereby reducing its height. As s is increased, the fringes are perturbed more strongly, because the condensate phase becomes less correlated at larger separations. The contrast therefore decreases faster with s than in the fully phase-coherent case. The greater the amplitude of the phase fluctuations, the faster the contrast decreases with s. Therefore by measuring the width of the correlation function at different temperatures, we extract the temperature dependence of the coherence length. Further information is obtained from the shape of the correlation function [33].

In the presence of phase fluctuations, each realization of the experiment gives a different interference pattern, even with fixed experimental conditions. Expression (2) must therefore be generalized to:

$$
C^{(1)}(s) = \int \mathrm{d}^3\mathbf{r} \left\langle \Psi_0^* \left(\mathbf{r} - \frac{s}{2}\mathbf{e}_z \right) \Psi_0 \left(\mathbf{r} + \frac{s}{2}\mathbf{e}_z \right) \right\rangle, \quad (3)
$$

where the brackets $\langle \rangle$ denote a statistical average of the random process describing the random phase. In practice, one must repeat the experiment at a given separation s and average the contrast measurements over many quasi-condensates to obtain $C^{(1)}(s)$.

This principle was used by Michelson in his famous astronomical interferometer, whose goal was to measure the spatial coherence of the light field arriving from a star, in order to deduce the diameter of the star [34]. However, Michelson's method is plagued by the existence of a randomly fluctuating relative phase between the two inputs

of the interferometer, and various methods insensitive to the relative phase fluctuations had to be developed [35]. A similar problem appears when one tries to determine the coherence length of a condensate or a quasi-condensate with interferometry. In addition to the controlled relative phase between the two components interfering in (1), there is an uncontrollable relative phase due to experimental problems such as a residual phase shift between the lasers creating the two copies or a random velocity kick imparted to the sample. In order to overcome this problem [36], Hellweg et al. [28] have used an analysis analogous to the Hanbury Brown and Twiss method [37], since it is based on the measurement of the second-order correlation function which is insensitive to global phase shifts. In contrast, our method is in line with the initial method of Michelson who could visually evaluate the contrast of the randomly moving fringes he was observing. The decrease of this contrast as a function of the telescopes' separation gave a direct measurement of the coherence length. Similarly, we directly evaluate the contrast of the fringes by taking the modulus of the Fourier transform of the fringe pattern. The decrease of that contrast as a function of the separation s yields the coherence length of the quasi-condensate.

3 Experiment

3.1 Creation of elongated Bose-Einstein condensates

In our experimental setup [38], a Zeeman-slowed atomic beam of ^{87}Rb is trapped in a MOT, and after optical pumping into the $5S_{1/2}|F = 1, m_F = -1\rangle$ state is transferred to a magnetic Ioffe-Pritchard trap created by an iron-core electromagnet. Our design allows us to lower the magnetic field at the bottom of the trap to a few Gauss and thus to obtain very tight radial confinement [39]. Using this trap, we are able to create condensates very close to the 1D Thomas-Fermi regime [40], as was demonstrated in [41–43]. In the present experiment, we produce condensates further into the 3D regime so that we can explore the cross-over regime ($T \sim T_\phi$). We use two different trap configurations: in the first, the final radial and axial trap frequencies are respectively $\omega_\perp = 2\pi \times 395$ Hz and $\omega_z = 2\pi \times 8.67$ Hz, giving an aspect ratio of 45; for the second trap configuration, the final frequencies are $\omega_\perp = 2\pi \times 655$ Hz and $\omega_z = 2\pi \times 6.55$ Hz, with aspect ratio 100. In this way, we obtain needle-shaped condensates containing around 3×10^5 atoms, with a typical half-length $L \simeq 85$ μm in the first trap and $L \simeq 120$ μm in the second. We control the final number of atoms by holding the condensate for a variable time, typically a few seconds, in the presence of an rf shield. The absolute number of atoms is calibrated from a measurement of the critical temperature, taking into account the effects of interactions [44]. For condensates with small condensate fractions (less than 60%), the temperature is obtained by fitting a Gaussian distribution to the thermal wings of the cloud. The temperature is then extrapolated from the final frequency of the rf ramp to lower temperatures for which the thermal fraction is indiscernible [43,45].
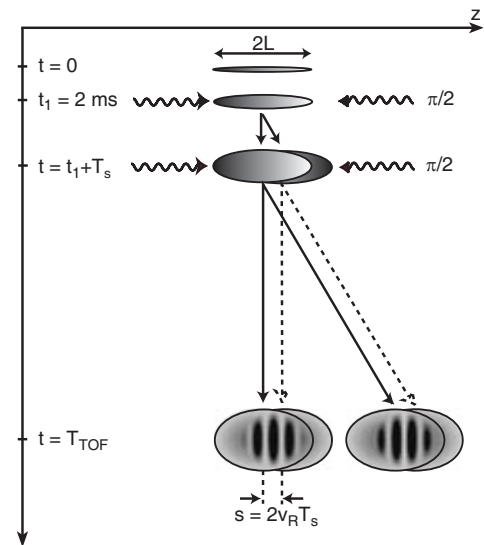

Fig. 1. The condensate is released from the trap at $t = 0$ and has a half-length of L. A sequence of two Bragg pulses is applied to generate the interferometer. Two output ports are created ($p = 0$, $p = 2\hbar k_L$) with complementary fringe patterns.

3.2 Interferometry set-up and timing

As shown in Figure 1, we implement the interferometer using a sequence of two $\frac{\pi}{2}$-Bragg pulses, which act as matter-wave beamsplitters. The set-up consists of two laser beams counter-propagating along the longitudinal trap axis, each of intensity ~ 2 mW cm^{-2}, red-detuned by $\Delta = 6.6$ GHz from the ^{87}Rb D2 line at $\lambda = 780.02$ nm. Two acousto-optic modulators driven by frequency synthesizers produce a small relative detuning δ, tuned to the two-photon Bragg resonance $\delta = 2\hbar k_L^2/m$, with m the atomic mass and $k_L = 2\pi/\lambda$. The momentum width along z of the expanding condensate corresponds to a frequency width of 200 Hz. Therefore we use Bragg pulses of ~ 100 μs, short enough such that the corresponding 1.6 kHz frequency width (full width at half maximum) is sufficient to couple the entire condensate. The thermal cloud surrounding the condensate has a momentum distribution with a frequency width ranging from 12 kHz to 60 kHz, much larger than that of the condensate. Thus, only a small fraction of the thermal cloud is coupled by the Bragg pulses [45]. By controlling the Bragg pulse length, we realize a $\frac{\pi}{2}$-pulse which splits the condensate into a coherent superposition of two wavepackets with velocities differing by $2v_R = 2\hbar k_L/m = 11.72$ mm s^{-1}, where v_R is the recoil velocity. The interferometer sequence is illustrated in Figure 1. The condensate is held in the trap for at least 2 s at the end of the final rf evaporative-cooling ramp, to allow residual oscillations to be damped [20,21]. After switching off the trap, the condensate is allowed to expand freely for 2 ms before the first $\frac{\pi}{2}$-pulse is applied. During this expansion the condensate density reduces by two orders of magnitude, so collisions between the diffracted wavepacket and the original condensate become negligible. During a free-evolution time 2 ms $< T_s <$ 10 ms, the two wavepackets
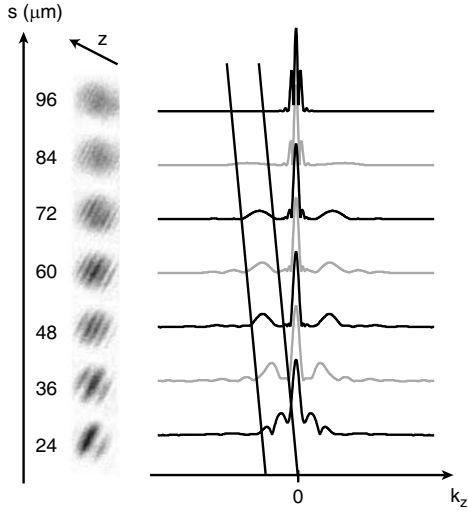
Fig. 2. Left: one of the two output ports of the interferometer for different separations s between the two condensate copies. The half-length of the initial condensate is $L = 85$ μm. Right: profiles of the 2D Fourier transform (absolute value) of each of the images on the left. The profiles are normalized to equal central peak height (proportional to total atom number). The position of the second peak (delimited by the two lines) gives the spatial frequency of the fringes, and the ratio of the height of the second peak to the central peak gives the fringe contrast.

separate to a distance $s = 2v_{\rm R}T_s$. The second $\frac{\pi}{2}$-pulse completes the interferometer, and we observe interference in each of the two output ports, which differ in momentum by $p = 2\hbar k_{\rm L}$. The condensate is imaged by absorption perpendicular to the long axis z after a 29 ms total time-of-flight [46].

For a given set of experimental conditions (condensate atom number and temperature), the experimental correlation function is acquired by taking a sequence of interference images with different condensate separations s ranging from $0.2L$ to $1.2L$, varied by changing T_s. For smaller separations, we do not observe enough fringes to obtain a reliable measurement of the contrast. At the maximum value of s, the contrast has reduced such that the fringes are no longer discernible above the noise. Typical images for $0.3L \leq s \leq 1.1L$ are shown in Figure 2. For each value of s, typically 5 images are taken, so that a statistical average can be performed. The fringe contrast is then measured, giving the correlation function. Correlation functions have been obtained at various temperatures T between 100 and 230 nK and for condensate atom numbers N_0 between 0.5×10^5 and 2.5×10^5. These conditions correspond to $0.8 < T/T_\phi < 8$, where $T_\phi = 15\hbar^2 N_0/16mL^2$ [27,47].

4 Analysis of interferograms

4.1 Interferogram

As shown in [25], a quasi-condensate is well-described by a fluctuating complex field $\Psi(\rho, z) = \sqrt{n(\rho,z)}{\rm e}^{i\Phi(\rho,z)}$,

with fixed density distribution $n(\rho, z)$ and fluctuating phase $\Phi(\rho, z)$. In the following, $\Psi(\rho, z)$ represents the wavefunction of the condensate after the free-fall expansion. The first Bragg pulse is applied after 2 ms of free expansion, at which time the density has reduced such that interactions between the atoms are negligible. We therefore assume that the different copies of the condensate propagate independently. The phase distribution can be expressed as $\Phi(\rho, z) = \alpha z^2 + \beta\rho^2 + \phi_{\rm th}(z)$, where $\phi_{\rm th}(z)$ represents the thermal phase fluctuations and the quadratic terms represent the parabolic phase developed during expansion.

We now consider the interference pattern produced at one of the output ports of the interferometer. For a separation s, we obtain the atomic density distribution:

$$n_{\rm out}(\rho, z) = \frac{1}{4}|\Psi(\rho, z - s/2) + \Psi(\rho, z + s/2)|^2$$
$$= \frac{n_+}{4} + \frac{n_-}{4} + \frac{\sqrt{n_+ n_-}}{2}\cos[\Delta\Phi(z) + \phi_{\rm g}], \quad (4)$$

with $n_\pm = n(\rho, z \pm s/2)$ and $\Delta\Phi(z) = \Phi(z + s/2) - \Phi(z - s/2)$. The global phase shift $\phi_{\rm g}$ is due to random, uncontrolled phase shifts between the two Bragg pulses. The phase difference between the two copies is $\Delta\Phi(z) = \alpha z s + \phi_{\rm th}(z + s/2) - \phi_{\rm th}(z - s/2)$. The density of the condensate is small when the first Bragg pulse is applied, so we neglect a small relative velocity due to repulsion between the two copies. At the second output port, the two condensate copies have an additional π relative phase shift due to the Bragg pulses, thereby producing a complementary fringe pattern. In our data analysis, the images of each output port are treated separately.

Since the global phase shift $\phi_{\rm g}$ fluctuates from shot to shot, we cannot average over different images at the same separation s. Instead, we take the contrast of each image individually and then average the contrast.

4.2 Analysis in Fourier space

The atoms are imaged by absorption along the vertical y-axis, perpendicular to the long axis of the trap. The image we obtain, rescaled to units of 2D atomic density, is the integrated density:

$$I(x, z) = {\rm const} \int {\rm d}y\, n_{\rm out}. \quad (5)$$

We take the 2D Fourier transform of this image and extract its profile along the zero radial frequency $k_x = 0$ axis:

$$\tilde{I}[0, k_z] = {\rm const} \int {\rm d}^3r\, n_{\rm out}e^{ik_z z}. \quad (6)$$

Typical images and their 2D Fourier transform profiles are shown in Figure 2 for different separations s. The contrast of the fringe pattern is given by the ratio $2\tilde{I}[0, k_0(s)]/\tilde{I}[0, 0]$, where $k_0(s) \simeq \alpha s$ is the dominant spatial frequency of the fringe pattern. The profiles of Figure 2 show clearly the increasing spatial frequency and decreasing contrast as a function of s.

To extract the correlation function, we take the complex amplitude of the Fourier peak at the spatial frequency k_0 of the fringes:

$$\tilde{I}[0, k_0(s)] = e^{i\phi_g} \int \mathrm{d}^3 r \, \sqrt{n_+ n_-} e^{i\Delta\Phi_{\mathrm{th}}}. \tag{7}$$

In the absence of the global phase shifts ϕ_g, the correlation function $C^{(1)}(s)$ would be obtained by taking the statistical average of equation (7):

$$C^{(1)}(s) = \left\langle \tilde{I}[0, k_0(s)] \right\rangle = \int \mathrm{d}^3 r \left\langle \sqrt{n_+ n_-} e^{i\Delta\Phi_{\mathrm{th}}} \right\rangle \tag{8}$$

which is identical to relation (3). However, ϕ_g changes from shot to shot and prevents us from averaging Fourier transforms directly in this way [48]. To eliminate this random phase, we can take the absolute value of the Fourier transform before averaging. Thus we obtain an effective correlation function:

$$C^{\mathrm{eff}}(s) = \left\langle \left| \tilde{I}[0, k_0] \right| \right\rangle = \left\langle \left| \int \mathrm{d}^3 r \, \sqrt{n_+ n_-} e^{i\Delta\Phi_{\mathrm{th}}} \right| \right\rangle. \tag{9}$$

Note that although it has similar behaviour, our effective correlation function is expected to be quantitatively different from $C^{(1)}(s)$. Taking the absolute value of the transform reduces the cancelling effect between the random thermal phase shifts in the statistical average, so that the effective correlation function $C^{\mathrm{eff}}(s)$ decays more slowly with s than $C^{(1)}(s)$, as calculated in the next section.

4.3 Simulation

The 1st order correlation function $C^{(1)}(s)$ can be calculated analytically [33], using the theory of [27] to account for the phase fluctuations. However, it is not possible to obtain an analytic expression for the effective correlation function $C^{\mathrm{eff}}(s)$ (Eq. (9)) which we measure. Therefore, to calculate $C^{\mathrm{eff}}(s)$, we first simulate the quasi-condensate phase fluctuations following the theory in [27]. The phase operator is given by:

$$\hat{\phi}_{\mathrm{th}}(\mathbf{r}) = [4n(\mathbf{r})]^{-1/2} \sum_j f_j^+(\mathbf{r})\hat{a}_j + h.c., \tag{10}$$

where $\hat{a}_j$ is the annihilation operator of the excitation with quantum number j. The solution of the Bogoliubov-de Gennes equations for "low energy" excitations (with energies $\epsilon_\nu < \hbar\omega_\perp$) gives the wavefunctions of these modes:

$$f_j^+(\mathbf{r}) = \sqrt{\frac{(j+2)(2j+3)gn(\mathbf{r})}{4\pi(j+1)R^2 L\epsilon_j}} P_j^{(1,1)}(z/L), \tag{11}$$

where $P_j^{(1,1)}$ are Jacobi polynomials, $g = 4\pi\hbar^2 a/m$ is the interaction strength, a is the scattering length, R and L are the size of the condensate in the trap and $\epsilon_j = \hbar\omega_z\sqrt{j(j+3)/4}$ is the energy of mode j [40]. We
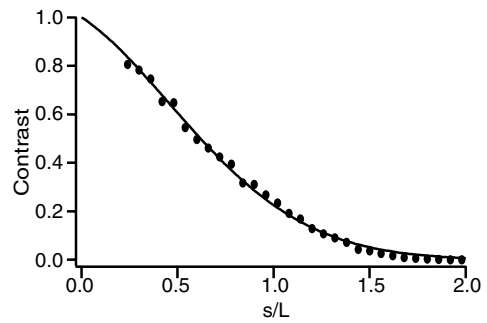

Fig. 3. Points represent the contrast extracted from our simulated absorption images (see text) as a function of s/L, L being the condensate half-length, for $T/T_\phi = 1$. These points are fitted by the product of a Gaussian and an exponential (solid line) which we take to be our theoretical effective correlation function $C^{\mathrm{eff}}(s)$.

assume the Thomas-Fermi approximation for the density $n(\mathbf{r})$, taking R and L from fits to images after expansion. To simulate numerically the phase fluctuations, we replace the operators $\hat{a}_j$ and $\hat{a}_j^\dagger$ by complex Gaussian random variables α_j and α_j^*. These variables have a mean value of zero and the correlation $\langle \alpha_j \alpha_{j'}^* \rangle = \delta_{jj'} N_j$ where $N_j = k_B T/(\hbar\omega_z\sqrt{j(j+3)/4})$ is the occupation number for the quasiparticle mode j at a given temperature T. We assume that the phase fluctuations do not evolve on the time scale of the expansion [33]. We have verified this by studying images of condensates after the same time-of-flight, but without the interferometer pulses. In this case, we observe a smooth density profile, with no extra features appearing in the Fourier transform.

For a given T/T_ϕ, 20 condensates are generated at each value of s, with s ranging from $0.2L$ to $2L$. Each condensate is integrated over y as in equation (5). These simulated absorption images are analysed in exactly the same way as the real experimental images. The absolute values of the Fourier transforms of the images are averaged, and the contrast extracted as in equation (9). The points in Figure 3 show the typical contrast extracted from our simulations for $T/T_\phi = 1$. We found that these points are very well fitted by the product of a Gaussian and an exponential, for all T/T_ϕ. We use these fits as our theoretical effective correlation functions $C^{\mathrm{eff}}(s)$.

The effective correlation function was simulated for $0 \leq T/T_\phi \leq 20$. Figure 4a presents results for different T/T_ϕ. At $T = 0$, $C^{\mathrm{eff}}(s)$ coincides with $C^{(1)}(s)$ [33]. This function is simply the integrated overlap function between the two condensates, and is approximately a Gaussian function of the separation s [32]. As T/T_ϕ increases, the width of the function decreases and its form gradually becomes exponential. In Figure 4b we plot the $1/e$ widths of the simulated $C^{\mathrm{eff}}(s)$ functions as a function of T/T_ϕ. For comparison we show also the width of $C^{(1)}(s)$ [33] which decreases much faster with T/T_ϕ.
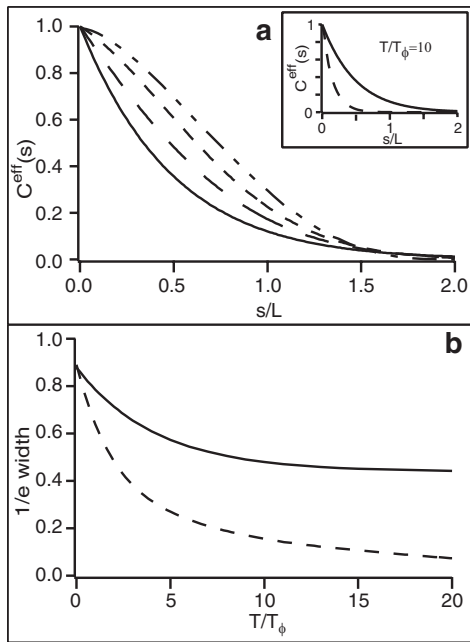
Fig. 4. Top: lines are simulated effective correlation function $C^{\mathrm{eff}}(s)$ (described in the text) as a function of s/L for different T/T_ϕ. From the top, $T/T_\phi = 0, 1, 3, 10$. With increasing T/T_ϕ, the curve changes from a quasi-Gaussian to an exponential and the width decreases. Inset: comparison of $C^{\mathrm{eff}}(s)$ (solid line) and $C^{(1)}(s)$ (dashed line) at $T/T_\phi = 10$. Bottom: width at $1/e$ of $C^{\mathrm{eff}}(s)$ (solid line) and $C^{(1)}(s)$ (dashed line) as a function of T/T_ϕ.

5 Experimental results

Figure 5 shows two examples of effective correlation curves measured using our interferometer and analysed as described above. The points shown in Figure 5a were obtained using a magnetic trap with an aspect ratio of 45, and with an atom number and temperature corresponding to $T/T_\phi = 1.35$, that is for small-amplitude phase fluctuations. The points in Figure 5b were obtained using a trapping aspect ratio of 100, and with $T/T_\phi = 4.86$. The contrast is plotted as function of s/L, obtained from a fit to a truncated parabola. Each point corresponds to an average over 5 condensates. The difference in the range of s/L explored is due to different expansion dynamics after release from the two different traps. In the more tightly confined trap (Fig. 5b), the axial expansion is much slower, and thus the fringe spacing decreases more slowly with s. At the smallest values of s, it is therefore impossible to measure the contrast reliably since we do not observe enough fringes. We can extract information about the phase fluctuations from both the shape and the width of these effective correlation functions.

5.1 Shape of the effective correlation functions

First, we observe qualitatively that the shape of the effective correlation functions $C^{\mathrm{eff}}(s)$ changes as T/T_ϕ increases. For small T/T_ϕ, as in Figure 5a, the curves are
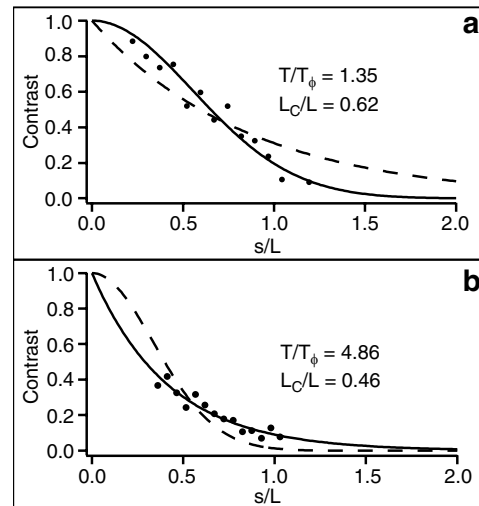

Fig. 5. Example of two experimental effective correlation profiles (points) as a function of s/L showing clearly the change in shape and width with T/T_ϕ. Each point is averaged over 5 condensates, each with 2 output port images. Top: at $T/T_\phi = 1.35$, the effective correlation curve is fitted by a Gaussian (solid line), with $1/e$ width $L_{\mathrm{C}}/L = 0.62$. The fit to an exponential (dashed line) is shown for comparison. Bottom: at $T/T_\phi = 4.86$, the effective correlation curve is fitted better by an exponential (solid line), with $1/e$ width $L_{\mathrm{C}}/L = 0.46$. The fit to a Gaussian (dashed line) is shown for comparison.

clearly Gaussian, as shown by the fit in the figure. As we increase T/T_ϕ, the profiles become rapidly exponential. We see in Figure 5b that at $T/T_\phi = 4.86$, the curve is already better fitted by an exponential than a Gaussian. At intermediate values of T/T_ϕ, we can use the product of a Gaussian and an exponential to fit a smooth curve through the data. The contribution of the exponential increases rapidly in importance at finite T, in agreement with the simulation, reflecting the increasing amplitude of the phase fluctuations with T/T_ϕ.

5.2 Comparison of coherence length L_{C}

In order to extract quantitative information from the effective correlation functions, we define a coherence length L_{C}, equal to the $1/e$ width of the effective correlation curve $C^{\mathrm{eff}}(s)$ [49]. We then use this parameter to compare the widths of the measured and simulated effective correlation functions. A smooth curve is fitted through the data (using the product of a Gaussian and an exponential) and the $1/e$ width extracted. Although the thermal cloud plays no role in the interference pattern we observe, it appears behind the condensates in the $p = 0$ output of the interferometer and thus reduces the measured contrast. Independent measurements of the thermal fraction (between 60% and 80% for this experiment) allow us to renormalize the experimental effective correlation functions to take account of this effect. When fitting the renormalized curves, we then fix the value at $s/L = 0$ to unity.
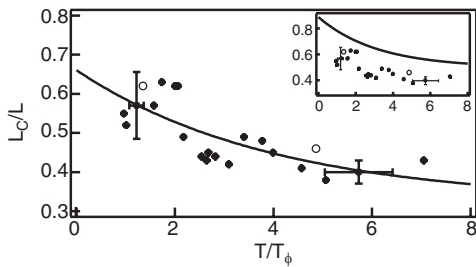
Fig. 6. L_C/L as a function of T/T_ϕ. The solid curve is a fit using an exponential with offset. Empty circles correspond to the two experimental correlation profiles of Figure 5. Error bars represent typical systematic errors. Inset: the solid curve is the simulated effective correlation function of Figure 4b.

In Figure 6, we plot L_C/L as a function of T/T_ϕ. Importantly, we see that the coherence length varies smoothly as a function of T/T_ϕ, even when the temperature is close to T_ϕ. This is what we should expect since T_ϕ is simply a characteristic temperature, defined as that at which the mean square fluctuations of the phase difference between two points separated by a distance L is equal to 1. Therefore it should be borne in mind that even condensates at temperatures below T_ϕ are not necessarily fully coherent.

The inset of Figure 6 compares the measured coherence widths with the results of the simulation (Fig. 4b). Despite the offset between the two curves, the trend of the data follows very well that of the simulation. To compare the decrease of the experimental and simulated coherence lengths, we fit the data by an exponential with an offset. The experimental coherence length decreases by 30(7)% between $T/T_\phi = 1$ and $T/T_\phi = 6$, in good agreement with the corresponding decrease of 28(1)% for the simulation. In the following discussion we consider possible explanations for the observed reduction in contrast.

5.3 Discussion

As shown in the inset of Figure 6, the measured coherence length is offset by about 25% from the results of the simulation at $T/T_\phi = 1$. In order to eliminate various possible causes of this discrepancy, and to understand better the limitations of our experiment, we have performed several tests.

Since the accuracy of our experiment relies on the comparison of fringe contrast at different spatial frequencies, it is important to take great care in setting up and characterising the imaging system. Therefore we measured the modulation transfer function (MTF) (see e.g. [50]) of our complete imaging system in situ, using a USAF1951 resolution target engraved with 3-bar square wave patterns of spatial frequency 4–200 lines/mm, covering the range of spatial frequencies observed in our interference experiment. By Fourier transforming images of different regions of the target, we were able to compare the magnitude of the different Fourier components in the image with those of the target pattern, thereby obtaining the MTF of our system.

We found that the MTF is approximately linear, falling from 1 at zero spatial frequency to 0 at 118 lines/mm. This resolution limit at 8.5 μm is in agreement with earlier characterisations of the system [42]. The shape of the MTF is due almost entirely to the CCD camera [51], and is surprisingly significant at fringe spacings much greater than the effective pixel size of 2.5 μm. All contrast measurements were corrected by this MTF. In fact, for the data obtained using the second trapping aspect ratio, the axial expansion (and thus the phase difference developed) was sufficiently small that the maximum observed fringe spatial frequency was 16 lines/mm and therefore the MTF correction had a negligible effect on the experimental effective correlation functions. In the first set of data, where the maximum fringe frequency was 38 lines/mm (a fringe spacing of 25 μm), the correction was more significant, changing the width of the curves by typically 10%, though still leaving a 20% discrepancy with the simulation.

We also considered the error introduced by a small focussing error. The imaging system is focussed onto the condensate to within ± 0.2 mm by minimising the imaged size of a small condensate as a function of the objective lens position. However, by varying the time-of-flight used, we may have introduced an error of up to ± 1 mm. Such an error could also be introduced by small changes to the residual magnetic fields, which lead to changes in the release velocity of the condensate when the magnetic trap is switched off. We measured effective correlation curves for different foci of the imaging system, but found that the width of the effective correlation curve changed by less than the existing spread in the points.

Other possible sources of error, such as the alignment of the imaging beam with respect to the condensates' fringes and correct background subtraction have also been eliminated. In Figure 6, we indicate the systematic errors for two points. These include calibration errors on the atom number and the image magnification. The uncertainty on the focussing adds a further error to L_C/L, which depends on the fringe spacing and thus on the axial trap frequency. These error bars show clearly that these systematic uncertainties are not sufficient to explain the discrepancy between the data and the theoretical prediction.

There remains in our experiment an unexplained phenomenon regarding the distribution of the fringe pattern. We expect to see fringes only in the region where the two condensates overlap. However, it can be seen in the images of Figure 7 that the fringes extend to the edges of each condensate. Moreover, these "extra" fringes have the same spatial frequency and phase as the central fringes. Although it is possible that a small fraction of the thermal cloud is coupled by the Bragg beams, interference fringes produced in this way [30] would have a much smaller fringe spacing, less than 6 μm. More importantly, the contributions from different parts of the original thermal cloud, whose width is ~ 100 μm, would sum incoherently to wash out the fringe pattern. It is more likely that these extra fringes arise as a result of interactions during the application of the Bragg pulses, but better modelling is still
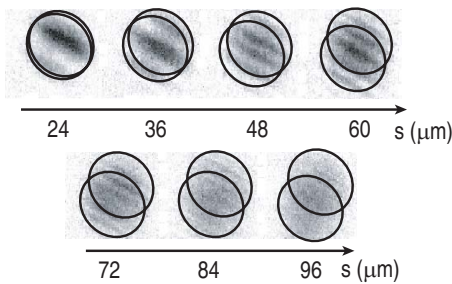
Fig. 7. Zoom on images of Figure 2. Circles represents the edge of the two condensates displaced by a distance s. The "extra" fringes are visible outside of the overlap region of the two condensates.

needed before evaluating whether their presence should increase or decrease the overall measured contrast.

6 Conclusion

We have demonstrated a new type of matter-wave interferometry using Bragg beam-splitter pulses and Fourier space analysis. Our results show that the expected shape of the correlation functions changes from a Gaussian-like shape to an exponential-like shape when the amplitude of phase fluctuations is increased. The coherence length of elongated condensates varies smoothly at temperatures close to T_ϕ, as predicted by theory. This highlights the fact that the characteristic phase temperature T_ϕ does not indicate a transition to full phase coherence, but rather that condensates exhibit phase fluctuations at all finite temperatures, albeit of small amplitude. This may place constraints on the trapping geometries which can be used for creating measurement devices based on the phase coherence of condensates.

References

1. M.H. Anderson et al., Science **269**, 198 (1995); K.B. Davis et al., Phys. Rev. Lett. **75**, 3969 (1995); C.A. Sackett, R.G. Hulet, Phys. Rev. Lett. **78**, 985 (1997); C.C. Bradley et al., Phys. Rev. Lett. **75**, 1687 (1995)
2. J. Reichel, W. Hänsel, T.W. Hänsch, Phys. Rev. Lett. **83**, 3398 (1999)
3. D. Müller, D.Z. Anderson, R.J. Grow, P.D.D. Schwindt, E.A. Cornell, Phys. Rev. Lett. **83**, 5194 (1999)
4. N.H. Dekker et al., Phys. Rev. Lett. **84**, 1124 (2000)
5. A. Haase, D. Cassettari, B. Hessmo, J. Schmiedmayer, Phys. Rev. A **64**, 043405 (2001)
6. J. Fortágh, H. Ott, G. Schlotterbeck, C. Zimmermann, Appl. Phys. Lett. **81**, 1146 (2002)
7. M.P.A. Jones, C.J. Vale, D. Sahagun, B.V. Hall, E.A. Hinds, Phys. Rev. Lett. **91**, 080401 (2003)
8. W. Hänsel, P. Hommelhoff, T.W. Hänsch, J. Reichel, Nature **413**, 498 (2001)
9. H. Ott, J. Fortágh, G. Schlotterbeck, A. Grossmann, C. Zimmermann, Phys. Rev. Lett. **87**, 230401 (2001)
10. T.L. Gustavson et al., Phys. Rev. Lett. **88**, 020401 (2002)
11. S. Schneider et al., Phys. Rev. A **67**, 023612 (2003)
12. Y. Lin, I. Teper, C. Chin, V. Vuletić, Phys. Rev. Lett. **92**, 050404 (2004)
13. J. Esteve, C. Aussibal, T. Schumm, C. Figl, D. Mailly, I. Bouchoule, C.I. Westbrook, A. Aspect, Phys. Rev. A **70**, 043629 (2004)
14. C. Vale, B. Upcroft, M.J. Davis, N.R. Heckenberg, H. Rubinsztein-Dunlop, J. Phys. B **37**, 2959 (2004)
15. E.A. Hinds, C.J. Vale, M.G. Boshier, Phys. Rev. Lett. **86**, 1462 (2001)
16. W. Hänsel, J. Reichel, P. Hommelhoff, T.W. Hänsch, Phys. Rev. A **64**, 063607 (2001)
17. E. Andersson, T. Calarco, R. Folman, M. Andersson, B. Hessmo, J. Schmiedmayer, Phys. Rev. Lett. **88**, 100401 (2002)
18. Y.-J. Wang et al., e-print arXiv:cond-mat/0407689
19. S. Dettmer et al., Phys. Rev. Lett. **87**, 160406 (2001)
20. I. Shvarchuck, Ch. Buggle, D.S. Petrov, K. Dieckmann, M. Zielonkowski, M. Kemmann, T.G. Tiecke, W. von Klitzing, G.V. Shlyapnikov, J.T.M. Walraven, Phys. Rev. Lett. **89**, 270404 (2002)
21. S. Richard, F. Gerbier, J.H. Thywissen, M. Hugbart, P. Bouyer, A. Aspect, Phys. Rev. Lett. **91**, 010405 (2003)
22. E.W. Hagley, L. Deng, M. Kozuma, M. Trippenbach, Y.B. Band, M. Edwards, M. Doery, P.S. Julienne, K. Helmerson, S.L. Rolston, W.D. Phillips, Phys. Rev. Lett. **83**, 3112 (1999)
23. J. Stenger et al., Phys. Rev. Lett. **82**, 4569 (1999)
24. I. Bloch, T.W. Hänsch, T. Esslinger, Nature **403**, 166 (2000)
25. D.S. Petrov, G.V. Shlyapnikov, J.T.M. Walraven, Phys. Rev. Lett. **85**, 3745 (2000)
26. Y. Castin, R. Dum, E. Mandonnet, A. Minguzzi, I. Carusotto, J. Mod. Opt. **47**, 2671 (2000)
27. D.S. Petrov, G.V. Shlyapnikov, J.T.M. Walraven, Phys. Rev. Lett. **87**, 050404 (2001)
28. D. Hellweg, L. Cacciapuoti, M. Kottke, T. Shulte, K. Sengstock, W. Ertmer, J.J. Arlt, Phys. Rev. Lett. **91**, 010406 (2003)
29. J.E. Simsarian, J. Denschlag, M. Edwards, C.W. Clark, L. Deng, E.W. Hagley, K. Helmerson, S.L. Rolston, W.D. Phillips, Phys. Rev. Lett. **85**, 2040 (2000)
30. D.E. Miller, J.R. Anglin, J.R. Abo-Shaeer, K. Xu, J.K. Chin, W. Ketterle, e-print arXiv:cond-mat/0412672
31. Y. Castin, R. Dum, Phys. Rev. Lett. **77**, 5315 (1996)
32. F. Zambelli, L. Pitaevskii, D.M. Stamper-Kurn, S. Stringari, Phys. Rev. A **61**, 063608 (2000)
33. F. Gerbier, J.H. Thywissen, S. Richard, M. Hugbart, P. Bouyer, A. Aspect, Phys. Rev. A **67**, 051602 (2003)

34. A.A. Michelson, Astroph. J. **51**, 257 (1920)
35. A. Labeyrie, in *Progress in Optics XIV*, edited by E. Wolf (North-Holland, 1976) pp. 47-87
36. Note that the Bragg momentum spectroscopy method does not suffer from this problem
37. R. Hanbury Brown, R.Q. Twiss, Nature **177**, 27 (1956); Nature **178**, 1046 (1956)
38. B. Desruelle et al., Phys. Rev. A **60**, R1759 (1999)
39. P. Bouyer, A. Aspect, M. Lécrivain, B. Desruelle, V. Boyer, patent 00 02704 (2000)
40. S. Stringari, Phys. Rev. A **58**, 2385 (1998)
41. P. Bouyer, J.H. Thywissen, F. Gerbier, M. Hugbart, S. Richard, J. Retter, A. Aspect, J. Phys. IV France **116**, 219 (2004)
42. S. Richard, Ph.D. thesis, University of Paris XI, 2003
43. F. Gerbier, Ann. Phys. Fr. **29**, no. 1 (2004)
44. F. Gerbier et al., Phys. Rev. Lett. **92**, 030405 (2004)
45. F. Gerbier, J.H. Thywissen, S. Richard, M. Hugbart, P. Bouyer, A. Aspect, Phys. Rev. A **70**, 013607 (2004)
46. Our cell allows maximum 25 ms free-fall. We increase the time-of-flight by applying, after the Bragg pulses, a magnetic field gradient opposed to the gravity field
47. In [27], T_ϕ is defined relative to a *phase coherence length* L_ϕ, such that $L_\phi/L = T_\phi/T$. Here, L_ϕ is the characteristic separation over which the phase fluctuates by 1 radian at the *trap centre*
48. This would be equivalent to averaging the original images: the fringe contrast would be averaged out to the non-interfering density profile
49. Note that this definition of L_C gives a value which is always smaller than L, even at $T = 0$, in contrast to the definition of L_ϕ which goes to infinity [47]. The $1/e$ values of both $C^{\text{eff}}(s)$ and $C^{(1)}(s)$ reflect the effects of both the phase fluctuations (characterised by L_ϕ) and the condensate density envelope $n(r)$. For $T/T_\phi > 8$, the phase fluctuations dominate and it was shown in [21,42,43] that the $1/e$ width of $C^{(1)}(s)$ is equivalent to αL_ϕ where the factor $\alpha = 0.64$ accounts for the fact that we integrate over the entire condensate, whereas L_ϕ is valid only at trap centre
50. J.W. Goodman, *Introduction to Fourier Optics*, 2nd edn. (McGraw-Hill, 1996)
51. This has been confirmed by MTF measurements of the Pixelfly HiRes camera alone, provided by PCO (www.pco.de)